Journal of Simulation and Analysis of Novel Technologies in Mechanical Engineering
16 (3) (2024) 0027~0040
DOI 10.71939/jsme.2024.1127451

Research article

Vibration and dynamic behavior of multi-layer sandwich composite piezoelectric micro beam using higher-order elasticity theory

Mehrdad Soltani[1,2], Javad Jafari Fesharaki[1,2], Seyed Ali Galehdari[1,2], Rasoul Tarkesh Esfahani[1,2] , Mohamad Shahgholi[1,2]

[1]*Department of Mechanical Engineering, Najafabad Branch, Islamic Azad University, Najafabad, Iran*
[2]*Modern Manufacturing Technologies Research center, Najafabad Branch, Islamic Azad University, Najafabad, Iran*

[*]jjafari.f@gmail.com

(Manuscript Received --- 28 July 2024; Revised --- 29 Nov. 2024; Accepted --- 17 Dec. 2024)

Abstract
Numerous scientists have examined the mechanical properties of materials at the micro- and nanoscale in recent years. Conversely, the remarkable advancements in micro and nanotechnology across several fields and industries, such as their extensive applications in micro- and nano-electro-mechanical systems (MEMS and NEMS), have piqued the curiosity of researchers. In this paper, vibration and dynamic behavior of multi-layer sandwich composite piezoelectric micro beam using higher-order elasticity theory by considering strain gradient and surface effects are investigated. The Hamilton's principle is utilized to derive the sandwich micro beam model with Gurtin- Murdoch surface theory and generalized differential quadrature method is used to discretize and solve the differential equation Moreover, the effects of higher order materials and geometry of model on control respond and frequency behavior have been presented. In addition, the role of different theories based FFT results has been examined. The results show that the small material length scale considering in the higher order theories plays a key role in the dynamic respond of models. Also, the result of higher order theories should be considered in micro and nano scale and the classical theory could not predict the mechanical behavior very well. The study's conclusions imply that the effectiveness of controller scheme is within the piezoelectric voltage range in terms of vibration control and feedback damping factors.

Keywords: Multi-Layer Sandwich Composite, Micro beam, higher-order elasticity theory, vibration and dynamic analysis

1- Introduction

The behavior of materials in the context of micro and nano electro-mechanical systems (MEMS and NEMS) has drawn the attention of numerous researchers in recent times. In many mechanical engineering applications, including atomic forces micro-scopes (AFMS), micro-switches, micro and nano sensors and actuators, micro rate gyros, and micro flexible joints, MEMS and NEMS play a significant role [1, 2]. Experimental studies have demonstrated that the size effect needs to be considered in the mechanical behavior of micro-scale structures when the length characteristic is on the order of microns [3]. Specifically, high longitudinal Young's modulus, strength to weight ratio, and high

frequency operation are unique characteristics that have drawn a lot of study from many scientific fields. Sandwich composite microstructures are a well-known class of small-scale materials with a wide range of uses in contemporary industries. The results of the experiments showed that the behavior of micro and nanomaterials differs fundamentally and is dependent on the structure's dimensions [4-6]. In order to address the fundamental drawbacks of classical theory, higher order continuum theories that take material length scale factors into account have been extended. Recent mechanical testing and experimental observations have made it clear that the behavior of materials at the micro and nanoscales essentially varies from that of materials at the macroscale and is strongly reliant on size as well as structure dimension [7-12]. Researchers have determined that the size impact needs to be considered in mechanical behavior in order to overcome this inherent weakness of classical theory and get the precise prediction of behavior in small-scale dimensions [13, 14]. As a result, several higher order continuum theories have been put forth that include factors related to the material length scale, such as strain gradient, Eringen, micropolar elasticity, couple stress, and modified couple stress. One of these advanced theories that many researchers have effectively used is the modified pair stress theory. Alashti et al. studied at the size-dependent behavior of microbeams in order to investigate static and free vibration problems utilizing the pair stress theory. The findings demonstrate that the deflection estimated by the previously indicated technique is less than that of the classical hypothesis [15]. Nikpourian and colleagues [16] report size-dependent nonlinear dynamic resonance of a piezoelectrically laminated MEMS. For both rectangular and circular micro-plates, Jomehzadeh et al. [17] provided a micro-mechanical study based on the modified couple stress for examining a wide range of length scale parameters, distinct aspect ratios, and alternative boundary conditions. Dynamic stability of manufactured double-sided NEMS with finite conductivity, surface energy, and nonlocal effect was achieved by Sedighi et al. [18]. Ding et al. [19] assessed the impact of the thickness, beam width, and electrode gap on the frequency response using a modified couple stress theory of electrostatically actuated micro-beam with von Kármán geometric nonlinearity. The dynamic behavior of geometrical imperfect micro-beam was studied by Farokhi et al. [20] taking into account the modified pair stress theory. To discretize the equation of motion, they used the Galerkin method. Sahmani and Bahrami [21] noted that the dynamic stability of micro-beams driven by piezoelectric voltage is depending on their size. A narrow elastic beam's bending and buckling were proven by Lazopoulos & Lazopoulos [22]. They came to the conclusion that when beam thickness decreased, so did the cross-section area's dependence, based on the strain gradient hypothesis. The increase in thin beam stiffness is responsible for this impact. Trindade and Benjeddou's finite element model [23] was created to assess the vibrational response of a traditional sandwich beam with a dynamic piezoelectric actuator and sensor. Ghaznavi et al. [24] examined the stability of transvers motion for a cantilever micro-beam integrated with piezoelectric layers for the actuator and sensor. Using strain gradient theory, Sahmani et al. [21] clarified the dynamic stability of a micro-beam driven by piezoelectric voltage.

Additionally, they contrasted the critical piezoelectric voltages predicted by the classical theory with those that included a range of length scale parameter values.

Researchers have been paying close attention to MEMS vibration abatement and control. Therefore, vibration control has made efficient use of a variety of control strategies. Based on the Strain Gradient nonlinear theory, Vatankhah et al. [25] examined a closed-loop control approach to reduce the vibration of a tiny Euler-Bernoulli cantilever beam utilizing linear piezoelectric actuation. Using the Galerkin projection approach, they transformed the controlling partial differential equation into a few ordinary differential equations, and a reliable linear controller was created for this model. Ansari et al.'s study included a computer analysis of Timoshenko nano-beam vibrations at various end conditions that took surface stress effects into account. They demonstrated how raising the dimensionless fundamental frequency is a direct result of raising the residual surface stress. The global dynamics and integrity of a micro-plate pressure sensor were expanded by Belarinelli et al. [26]. Gurtin-Murdoch elasticity theory was utilized by Mohammadimehr et al. [27] to examine the influence of surface effects on the free vibration of an isotropic piezoelectric Timoshenko micro-beam. Their research demonstrated how the natural frequency responses are impacted by surface stress effects. The Gurtin–Murdoch surface stress and strain gradient theory was utilized by Mirkalantari et al. [28] to forecast the pull-in instability behavior of nano-plates. They employed the GDQM to solve governing equations in their research.

To the best of the author's knowledge, no research has been published on the best wy to control a microbeam using piezoelectric layers based on modified couple stress the ory. The majority of related studies in micr o and nano mechanical behavior that take i nto account higher order continuum theorie s concentrated on size dependent effect, sta bility, and vibration analyses of the model. Furthermore, sandwich structures with piez oelectric layers in micro scale that take surf ace stress elasticity into account have recei ved much too little attention.

Surface stress elasticity and higher order elasticity theory are used to model the structure of micro cantilever beam model in the current study. Based on Hamilton's principle, the governing equations of motion and boundary conditions for a multilayer piezoelectric and micro-beam are constructed, and GDQM is then used to discretize the data. The LQR with output feedback is utilized to assess the active vibration control capability.

2- Governing equations of motion

Composite cantilever sandwich microbeam with two active silicon material qualities with PZT-4 piezoelectric layers linked to a thick porous core constitutes the fundamental idea of the problem. This sophisticated, one-of-a-kind structure was developed using surface stress and strain gradient theories.

A schematic of a micro cantilever beam integrated with piezoelectric layers is presented in Figure 1. The length and width of the microbeam in this model are L and b, respectively. Furthermore, two thickness parameters related to the bulk and piezoelectric thickness, respectively, are indicated by h_b and h_p [29].

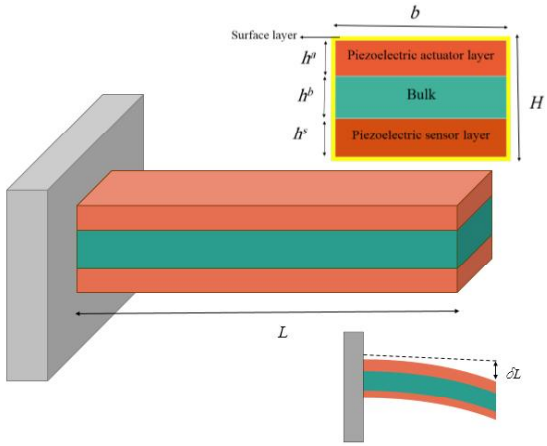

Fig. 1 Schematic of micro cantilever beam with piezoelectric layers[30]

The displacement field of an Euler-Bernoulli beam is stated as [31]:

$$U_1 = -Z\frac{\partial w(X,t)}{\partial X} \tag{1}$$

$$U_2 = 0$$
$$U_3 = w(X,t)$$

where U_1, U_2 and U_3 directions are denoted by the letters in X, Y and Z, respectively. The potential strain energy without surface effect is extracted as [27]:

$$U = \int_{\Omega}^{\cdot}(\sigma_{ij}\,\varepsilon_{ij} + P_i\gamma_i + \tau_{ijk}^{(1)}\eta_{ijk}^{(1)} + m_{ij}x_{ij} - D_iE_i)dV \tag{2}$$

where σ_{ij} and ε_{ij} are Cauchy stress and strain tensors which are defined as Eqs. (3) and (4), respectively [32].

$$\sigma_{ij} = \lambda\delta_{ij}\varepsilon_{mm} + 2\mu\varepsilon_{ij} - e_{nij}E_n \tag{3}$$

$$\varepsilon_{ij} = \frac{1}{2}(u_{i.j} + u_{j.i}) \tag{4}$$

In which λ and μ are the Lame constants, e and $\delta_{ij}$are the piezoelectric coefficient and kronecker delta.

The material length scale parameters are presented in follows equations where m_{ij}, x_{ij} , D_i and E_i denote the deviatoric part of couple stress tensor, symmetric curvature tensor, electrical displacement and electrical field, respectively which are given as Eqs. (5)-(8) [32]:

$$m_{ij} = 2\mu l_2^2\chi_{ij} \tag{5}$$

$$\chi_{ij} = \frac{1}{2}(\theta_{i,j} + \theta_{j.i}) \tag{6}$$

$$D_i = e_{imn}\varepsilon_{mm} + \epsilon_{im}E_m \tag{7}$$

$$E_i = -\Phi_{,i} \tag{8}$$

where θ, ϵ, $\Phi_{,i}$, μ and l_2 are the infinitesimal rotation vector, the dielectric permittivity constant, the electric potential, shear modulus and length scale parameter associated with symmetric rotation gradients, respectively. The Rotation vector is considered as Eq. (9) [21]:

$$\theta_i = \frac{1}{2}curl(u_{i.j}) \tag{9}$$

and the higher order parameters can be obtained as follow:

$$\chi_{12} = \chi_{21} = -\frac{1}{2}\frac{\partial^2 w}{\partial x^2} \tag{10}$$

$$\gamma_1 = \varepsilon_{11,1} = -Z\frac{\partial^3 w}{\partial x^3}$$
$$\gamma_3 = \varepsilon_{11,3} = -\frac{\partial^2 w}{\partial x^2} \tag{11}$$

$$\eta_{113}^{(1)} = \eta_{131}^{(1)} = \eta_{311}^{(1)} = -\frac{4}{15}\frac{\partial^2 w}{\partial x^2}$$
$$\eta_{111}^{(1)} = -\frac{2}{5}Z\frac{\partial^3 w}{\partial x^3}$$
$$\eta_{333}^{(1)} = \frac{1}{5}\frac{\partial^2 w}{\partial x^2} \tag{12}$$
$$\eta_{223}^{(1)} = \eta_{232}^{(1)} = \eta_{322}^{(1)} = \frac{1}{15}\frac{\partial^2 w}{\partial x^2}$$
$$\eta_{122}^{(1)} = \eta_{212}^{(1)} = \eta_{221}^{(1)} = \eta_{133}^{(1)} = \eta_{331}^{(1)} = \eta_{313}^{(1)} = \frac{1}{5}Z\frac{\partial^3 w}{\partial x^3}$$

The higher-order stresses defined as [33] and [34]:

$$m_{12}^B = m_{21}^B = -\mu l_2^2\frac{\partial^2 w}{\partial x^2}$$
$$m_{12}^P = m_{21}^P = -\mu l_2^2\frac{\partial^2 w}{\partial x^2} \tag{13}$$

$$p_1^B = -2\mu l_0^2 Z\frac{\partial^3 w}{\partial x^3} \tag{14}$$

$$p_3^B = -2\mu l_0^2\frac{\partial^2 w}{\partial x^2}$$
$$p_1^P = -2\mu l_0^2 Z\frac{\partial^3 w}{\partial x^3}$$
$$p_3^P = -2\mu l_0^2\frac{\partial^2 w}{\partial x^2} \tag{15}$$

$$\tau_{113}^{B(1)} = \tau_{131}^{B(1)} = \tau_{311}^{B(1)} = -\frac{8}{15}\mu l_1^2\frac{\partial^2 w}{\partial x^2} \tag{16}$$

$$\tau_{111}^{B(1)} = -\frac{4}{5}\mu l_1^2 Z\frac{\partial^3 w}{\partial x^3}$$
$$\tau_{333}^{B(1)} = \frac{2}{5}\mu l_1^2\frac{\partial^2 w}{\partial x^2}$$
$$\tau_{223}^{B(1)} = \tau_{232}^{B(1)} = \tau_{322}^{B(1)} = \frac{2}{15}\mu l_1^2\frac{\partial^2 w}{\partial x^2}$$
$$\tau_{122}^{B(1)} = \tau_{212}^{B(1)} = \tau_{221}^{B(1)} = \tau_{133}^{B(1)} = \tau_{331}^{B(1)} = \tau_{313}^{B(1)} = \frac{2}{5}\mu l_1^2 Z\frac{\partial^3 w}{\partial x^3}$$
$$\tau_{122}^{P(1)} = \tau_{212}^{P(1)} = \tau_{221}^{P(1)} = \tau_{133}^{P(1)} = \tau_{331}^{P(1)} = \tau_{313}^{P(1)} = \frac{2}{5}\mu l_1^2 Z\frac{\partial^3 w}{\partial x^3}$$
$$\tau_{223}^{P(1)} = \tau_{232}^{P(1)} = \tau_{322}^{P(1)} = \frac{2}{15}\mu l_1^2\frac{\partial^2 w}{\partial x^2}$$
$$\tau_{333}^{P(1)} = \frac{2}{5}\mu l_1^2\frac{\partial^2 w}{\partial x^2} \tag{17}$$
$$\tau_{113}^{P(1)} = \tau_{131}^{P(1)} = \tau_{311}^{P(1)} = -\frac{8}{15}\mu l_1^2\frac{\partial^2 w}{\partial x^2}$$
$$\tau_{111}^{P(1)} = -\frac{4}{5}\mu l_1^2 Z\frac{\partial^3 w}{\partial x^3}$$

The distribution of electrical potential across the thickness of the piezoelectric micro-layer is represented by the equation (Eq). (18) [32]:

$$\Phi^{(p)}(x,z,t) = -\cos(\beta z)\phi\,(x,t) + \frac{2zV_0}{h^{(p)}} \tag{18}$$

$\beta = {}^{\pi}/_{h_p}$ and V_0 is the external electric voltage. The surface stress theory can be achieved as:[28, 35]:

$$U_s = \frac{1}{2}\int_0^L \oint_{\partial A} (\tau_{ij}\,\varepsilon_{ij} + \tau_{ni} u_{n,i}) \tag{19}$$

and τ^s is the residual surface stress under uncertain condition and $\tau_{\alpha\beta}$ is the in-plane components of surface stress tensor λ^s and μ^s are surface elastic constants which are assumed as follows [27]:

$$\lambda^s = \frac{E^s \upsilon^S}{(1+\upsilon^S)(1-2\upsilon^S)} \tag{20}$$

$$\mu^s = \frac{E^s}{2(1+\upsilon^S)} \tag{21}$$

where υ^S and E^s are Poisson's ratio and Young's modulus, respectively.

The kinetic energy of the model can be written as:

$$\begin{aligned} T^{(B)} &= \frac{1}{2}\int_0^L \left\{ I_0^{(b)} \left(\frac{\partial w}{\partial t}\right)^2 + I_2^{(b)} \left(\frac{\partial^2 w}{\partial x \partial t}\right)^2 \right\} dx \\ T^{(A)} &= \frac{1}{2}\int_0^L \left\{ I_0^{(a)} \left(\frac{\partial w}{\partial t}\right)^2 + I_2^{(a)} \left(\frac{\partial^2 w}{\partial x \partial t}\right)^2 \right\} dx \\ T^{(S)} &= \frac{1}{2}\int_0^L \left\{ I_0^{(s)} \left(\frac{\partial w}{\partial t}\right)^2 + I_2^{(s)} \left(\frac{\partial^2 w}{\partial x \partial t}\right)^2 \right\} dx \end{aligned} \tag{22}$$

in which the moment of inertia can be obtained as follows:

$$\begin{aligned} I_0^{(B)} &= \int_{A^{(B)}} \rho_b \, dA^{(b)}, \; I_2^{(B)} = \int_{A^{(B)}} \rho_b Z^2 \, dA^{(B)} \\ I_0^{(A)} &= \int_{A^{(A)}} \rho_a \, dA^{(A)}, \; I_2^{(A)} = \int_{A^{(P)}} \rho_a Z^2 \, dA^{(A)} \\ I_0^{(S)} &= \int_{A^{(s)}} \rho_s \, dA^{(S)}, \; I_2^{(P)} = \int_{A^{(S)}} \rho_s Z^2 \, dA^{(S)} \end{aligned} \tag{23}$$

ρ_b, ρ_a and ρ_s denote the densities of the bulk and piezoelectric layers including the actuator and sensor, respectively. By considering the kinetic energy and strain energy we have:

$$\Pi = U^{total} - T^{total} \tag{24}$$

Π is the total potential energy of model Therefore, Hamilton's principle and variational method can be explained by:

$$\delta \int_{t_1}^{t_2} \left(U^{total} - T^{total}\right) dt = 0 \tag{25}$$

generates the following partial differential equations of motion for the integrated micro-beam with piezoelectric layers, the final equations of motion can be expressed as:

$$\delta w: \frac{1}{2} bE^b \left[\frac{h_0^3}{12}\right] + \frac{1}{2} C_{11}^{(a)} b \left[\frac{\left(\frac{h_0}{2}+h^{(a)}\right)^3}{3} - \frac{\left(\frac{h_0}{2}\right)^3}{3}\right] +$$

$$\delta w: \frac{1}{2} bE^b \left[\frac{h_0^3}{12}\right]$$
$$+ \frac{1}{2} C_{11}^{(a)} b \left[\frac{\left(\frac{h_0}{2}+h^{(a)}\right)^3}{3} - \frac{\left(\frac{h_0}{2}\right)^3}{3}\right]$$
$$+ \frac{1}{2} C_{11}^{(s)} b \left[\frac{\left(-\frac{h_0}{2}\right)^3}{3} - \frac{\left(-\frac{h_0}{2}-h^{(s)}\right)^3}{3}\right]$$
$$+\mu^{(s)} l_2^2 A^{(s)} + \mu^{(a)} l_2^2 A^{(a)} + \mu^{(b)} l_2^2 A^{(b)}$$
$$+ 2\mu^{(b)} l_0^2 A^{(b)} + 2\mu^{(a)} l_0^2 A^{(a)} + 2\mu^{(s)} l_0^2 A^{(s)}$$
$$+ \frac{8}{15}\mu^{(b)} l_1^2 A^{(b)} + \frac{8}{15}\mu^{(a)} l_1^2 A^{(a)}$$
$$+ \frac{8}{15}\mu^{(s)} l_1^2 A^{(s)} + E^{s(a)} \frac{h^2}{4} b$$
$$+ 2\left(-\frac{h_0^3}{24} + \frac{h^3}{24}\right) E^{s(a)} + E^{s(a)} \frac{h_0^2}{4} b$$
$$+ E^{s(b)} b \frac{h_0^2}{2} + E^{s(b)} \frac{h_0^3}{6} + E^{s(s)} \frac{h^2}{4} b$$
$$+ 2\left(-\frac{h^3}{24} + \frac{h_0^3}{24}\right) E^{s(s)} + E^{s(s)} \frac{h_0^2}{4} b \left(\frac{\partial^4 w}{\partial x^4}\right)$$
$$\left(-2\mu^{(a)} l_0^2 I^{(a)} - 2\mu^{(s)} l_0^2 I^{(s)} - 2\mu^{(b)} l_0^2 I^{(b)}\right.$$
$$- \frac{4}{5}\mu^{(b)} l_1^2 I^{(b)} - \frac{4}{5}\mu^{(a)} l_1^2 I^{(a)}$$
$$\left.- \frac{4}{5}\mu^{(s)} l_1^2 I^{(s)}\right) \left(\frac{\partial^6 w}{\partial x^6}\right)$$
$$+ \left(\frac{1}{2} e_{31} b \left[\frac{1}{\beta}\left(\left(\cos\left(\beta\left(\frac{h_0}{2}+h^{(a)}\right)\right)\right.\right.\right.\right.$$
$$\left.\left.\left.\left.- \cos\left(\beta \frac{h_0}{2}\right)\right)\right)\right.$$
$$+ \left(\frac{h_0}{2}\right.$$
$$\left.\left.+ h^{(a)}\right)\left(\sin\left(\beta\left(\frac{h_0}{2}+h^{(a)}\right)\right)\right) - \left(\frac{h_0}{2}\right)\sin\left(\beta\frac{h_0}{2}\right)\right]$$
$$+ \frac{1}{2} e_{31}^{s(a)} b\beta \left(-\frac{h}{2}\right)\cos\left(-\frac{h}{2}\beta\right)$$
$$+ e_{31}^{s(a)} \left[\frac{1}{\beta}\cos\left(-\frac{h_0}{2}\beta\right) - \frac{h_0}{2}\sin\left(-\beta\frac{h_0}{2}\right)\right.$$
$$\left.- \frac{1}{\beta}\cos\left(-\frac{h}{2}\beta\right) + \frac{h}{2}\sin\left(-\beta\frac{h}{2}\right)\right]$$
$$\left.+ \frac{1}{2} e_{31}^{s(a)} (b) \left(-\frac{h_0}{2}\right)\beta\cos\left(-\frac{h_0}{2}\beta\right)\right)\left(\frac{\partial^2 \phi^{(a)}}{\partial x^2}\right)$$
$$+ \left(\frac{1}{2} e_{31} b \left[\frac{1}{\beta}\left(\cos\left(-\beta\frac{h_0}{2}\right)\right.\right.\right.$$
$$\left.- \cos\left(\beta\left(-\frac{h_0}{2}-h^{(s)}\right)\right)\right)$$
$$- \left(\frac{h_0}{2}\right)\sin\left(-\beta\frac{h_0}{2}\right) + \left(\frac{h_0}{2}\right.$$
$$\left.\left.\left.+ h^{(s)}\right)\left(\sin\left(\beta\left(-\frac{h_0}{2}-h^{(s)}\right)\right)\right)\right]$$
$$+ \frac{1}{2} e_{31}^{s(s)} b\beta \left(\frac{h}{2}\right)\cos\left(\frac{h}{2}\beta\right)$$
$$+ e_{31}^{s(s)} \left[\frac{1}{\beta}\cos\left(\frac{h}{2}\beta\right) + \frac{h}{2}\sin\left(\beta\frac{h}{2}\right) - \frac{1}{\beta}\cos\left(\frac{h_0}{2}\beta\right)\right.$$
$$\left.- \frac{h_0}{2}\sin\left(\beta\frac{h_0}{2}\right)\right]$$
$$\left.+ \frac{1}{2} e_{31}^{s(s)} b \left(\frac{h_0}{2}\right)\beta\cos\left(\frac{h_0}{2}\beta\right)\right)\left(\frac{\partial^2 \phi^{(S)}}{\partial x^2}\right)$$
$$+ \left(-\rho^{(a)} I^{(a)} - \rho^{(S)} I^{(S)} - \rho^{(b)} I^{(b)}\right)\left(\frac{\partial^4 w}{\partial x^2 \partial t^2}\right)$$
$$+ \left(\rho^{(a)} A^{(a)} + \rho^{(s)} A^{(s)} + \rho^{(b)} A^{(b)}\right)\left(\frac{\partial^2 w}{\partial t^2}\right) = 0 \quad (26)$$

The boundary conditions of micro cantilever beam are obtained from Eq. (28):

$$w(0) = 0 \tag{27}$$

$$\frac{\partial w(0)}{\partial x} = 0$$

$$\frac{\partial^2 w(L)}{\partial x^2} = 0$$

$$\frac{\partial^3 w(L)}{\partial x^3} = 0$$

3- Solution and discretization

To discretize the governing equations derived, the generalized differential quadrature method (GDQM) is used [36, 37]. GDQM is an advanced numerical technique employed to describe the flexural and longitudinal free vibrations of the model. This method is applied to convert the partial differential equation into an ordinary differential equation. In GDQM, the derivative of a function is approximated by a weighted linear sum of function values at specified grid points along the coordinate direction. According to this method, the partial derivatives of a function f at a point x_i are obtained as [6, 38]:

$$f^{(r)}(x_i) = \sum_{i=1}^{N} C_{ij}^{(r)} f(x_i)\,, \quad i = 1, 2, \dots, N \tag{28}$$

Using stiffness matrices [K], mass matrices [M], and the Rayleigh damping matrix [C], respectively, the discretized Eq. (29) and the associated boundary conditions can be expressed as matrices [29, 39]

$$\left([M]\{\ddot{X}\} + [C]\{\dot{X}\} + [K]\{X\}\right) = \{F\} \tag{29}$$

$$[C] = \alpha_1\,[M] + \alpha_2\,[K]$$

$$\left(\begin{bmatrix} M^{ww} & 0 & 0 \\ 0 & 0 & 0 \\ 0 & 0 & 0 \end{bmatrix} \begin{Bmatrix} \ddot{W} \\ \ddot{\Phi}_{(a)} \\ \ddot{\Phi}_{(s)} \end{Bmatrix} + \begin{bmatrix} C^{ww} & C^{w\Phi_{(a)}} & C^{w\Phi_{(s)}} \\ C^{\Phi_{(a)}w} & C^{\Phi_{(a)}\Phi_{(a)}} & C^{\Phi_{(a)}\Phi_{(s)}} \\ C^{\Phi_{(s)}w} & C^{\Phi_{(s)}\Phi_{(a)}} & C^{\Phi_{(s)}\Phi_{(s)}} \end{bmatrix} \begin{Bmatrix} \dot{W} \\ \dot{\Phi}_{(a)} \\ \dot{\Phi}_{(s)} \end{Bmatrix} + \begin{bmatrix} K^{ww} & K^{w\Phi_{(a)}} & K^{w\Phi_{(s)}} \\ K^{\Phi_{(a)}w} & K^{\Phi_{(a)}\Phi_{(a)}} & 0 \\ K^{\Phi_{(s)}w} & 0 & K^{\Phi_{(s)}\Phi_{(s)}} \end{bmatrix} \begin{Bmatrix} W \\ \Phi_{(a)} \\ \Phi_{(s)} \end{Bmatrix} \right) = \begin{Bmatrix} P \\ F_{(a)} \\ 0 \end{Bmatrix} \tag{30}$$

4- Results and discussion

This section examines the effects of a number of parameters on an integrated cantilever micro beam based on modified couple stress continuum theory, including thickness to material length scale parameter ratio, surface residual stress, Young's modulus of surface layer, surface mass density, and surface piezoelectric constant.

When a structure undergoes mechanical or thermal oscillations, its deformation can be measured by detecting the induced electric charges in the sensor layer. The resulting output voltage is supplied to the actuator, which can be regulated using a closed-loop control algorithm that responds to deformation or strain inputs. By integrating distributed piezoelectric sensors and actuators, the generated force can mitigate structural vibrations and prevent resonance. This approach, implemented via a piezoelectric micro-beam, is used to control vibration, buckling, shape, damage assessment, and active noise in microstructures.

Table 1 represents the mechanical and geometrical characteristics of bulk and piezoelectric layers. [21].

Table 1: The geometric and material constant of the micro-beam and piezoelectric layer.

Parameters	Bulk	Piezoelectric layer
Thickness(μm)	3	3
Length(μm)	450	450
Width(μm)	50	50
Young's modulus (Gpa)	210	64
Mass density(Kg/m^3)	2331	7500
Poisson's ratio	0.24	0.27
$e_{31}(C/m^2)$	-	-10
$(C^2/m^2\,N)\epsilon_{33}$	-	1.0275×10^{-8}
$l\ (\mu m)$	17.6	17.6

Based on the classical continuum theory, Fig. 2 shows the GDQM accuracy of the model for the first two vibrational modes of the cantilever micro-beam combined with piezoelectric layers. It is evident that as the number of grid points rises, so does the precision of the vibrational modes. Furthermore, it is demonstrated that the boundary conditions connected with the model exhibit a good degree of consistency in the geometry of the vibration modes. Although, increasing the number of grid point enhanced the prediction of model, finding the best number of points should be considered.

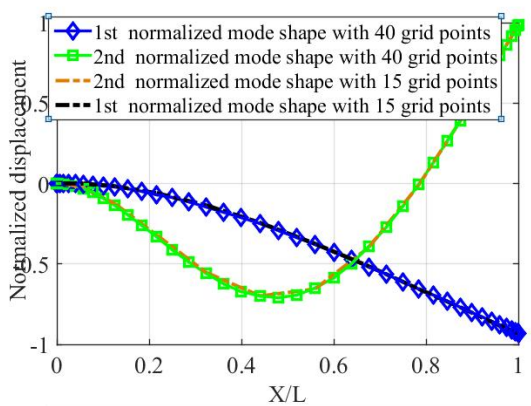

Fig. 2 Comparison of normalized vibrational mode shapes of the cantilever micro-beam with different number of grid points.

Fig.3. illustrated the natural frequency fluctuation versus thickness at various beam lengths and thicknesses. In order to study the natural frequency, the thickness of all layers both bulk and piezoelectric is taken to be constant. Following the demonstration of the convergence and accuracy of the approaches, a series of size-dependent studies were carried out in order to elucidate the effects of surface stress, geometry, and independent material length scale effects in addition to other parameters on the cantilever micro sandwich beam's natural frequencies and dynamic response. The thickness effects the first natural frequency for various beam lengths are displayed in Fig. 3. In this simulation, various length scales have been compared. It has been noted that natural frequencies decrease when L/H ratios rise. The increasing length to thickness ratios makes this phenomenon more prominent. This figure also show that thickness dimensions have a significant impact on natural frequency in comparison to length.

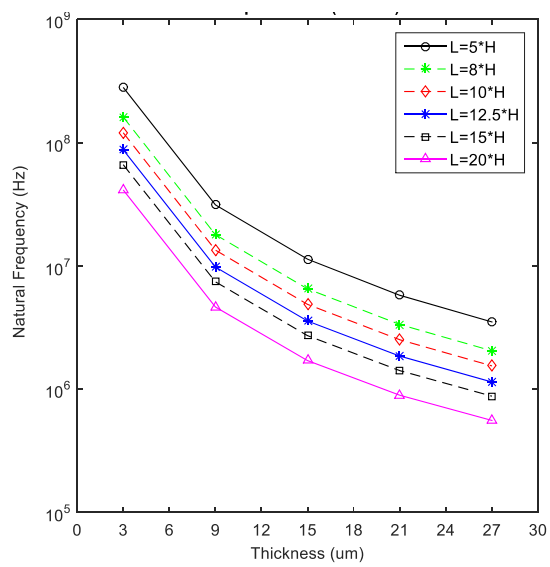

Fig. 3 L/H effects on the natural frequency of model

Based on strain gradient theory, Fig. 4 shows how the material length scale parameter l_0 linked to dilatation gradient affects the fundamental natural frequency of cantilever microbeams at different thicknesses and lengths. It is concluded that, in comparison to the other parameters, the influence of material

lengths scale parameter l_0 on the vibration of frequency is more important.

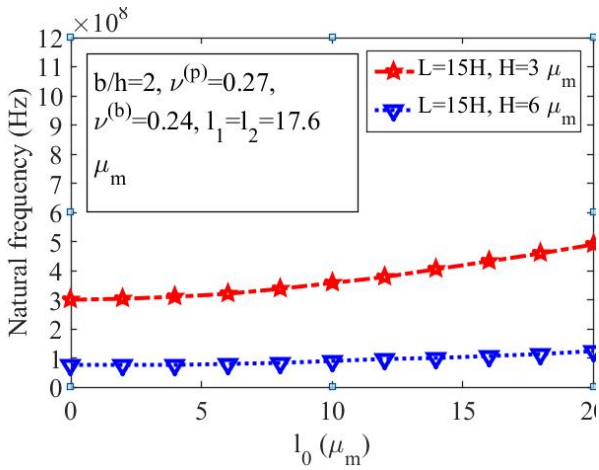

Fig. 4 Effect of length scale parameter l_0 on natural frequency of model

The impact of the material length scale parameter l_2, which is associated with symmetric rotation, on the first natural frequency as a function of different lengths to thickness ratios is displayed in Figure 9. Figure 5 makes it clear that a rise in the material length scale parameter l_2 corresponds to an increase in the natural frequency's magnitude. Furthermore, a decrease in the fundamental natural frequency is observed with an increase in the length ratio; this decrease is ascribed to the model's reduced stiffness matrix. At smaller thicknesses, the impact of the material length scale parameters l_2 becomes more significant. It good to mentioned that this parameters related to SGT and leads to predict the results of model precisely.

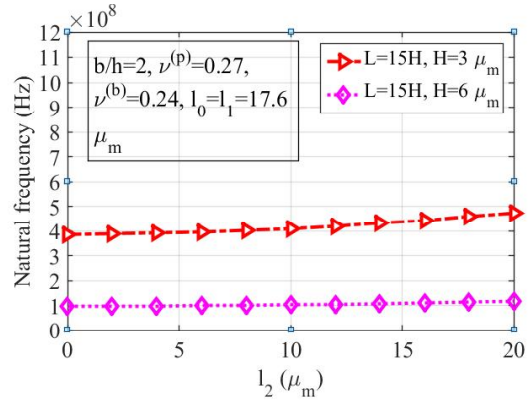

Fig. 5 Effect of length scale parameter l0 on natural frequency of model

The initial tip displacements of magnitude 5% of the model length are subjected to in order to obtain the vibrational response of the micro-beam model. In this instance, structural dampening is neglected because the focus was on determining whether the suggested approach could be implemented and how well the dynamic behavior performed. Fig. 5 provides the corresponding tip displacement for each of the classical and higher-order models. The vertical axes represent expansions for the model's tip deflection in meters, while the horizontal y-axis indicates the simulation period in seconds.

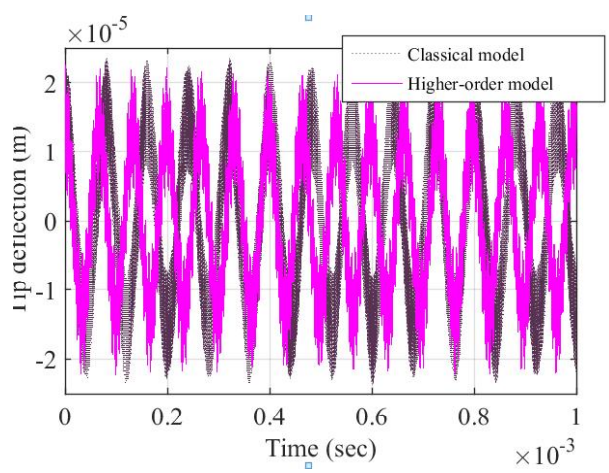

Fig. 6 Dynamic response comparison of classical and higher order models

Another aspects of dynamic response can be consider based on control behavior of system. To this end, response of model to LQR controller has been simulated. In which the following equation can be expressed the controller relation:

$$J = \int_0^{\infty} (\{y\}^T [Q]\{y\} + \{V_a\}^T [R]\{V_a\})\, dt \quad (31)$$

where $[Q]$ and $[R]$ are a symmetric matrix for the control performance and control cost. The $R = rI$

In this technique, a tip displacement of 5% of the microbeam length is taken into account for the initial condition. Low magnitude is produced by the sensor's piezoelectric bending after micro-beam deflection. While an optimal control gain is computed to minimize an objective function, the LQR controller is regulated to process the input signal. Ultimately, the actuator layer's control voltage has the ability to reduce the vibration of the microbeam. The weighting factor R role is examined in Fig. 7 with the assumption that q = 5. It is demonstrated that the bigger values for the amplitude response for the micro-beam model are recreated by raising the weighting factor. The tip deflection suppressed by LQR control becomes worse than that of the lowest weighting factor R control because the weighting factor R control will increase the overshoot action.

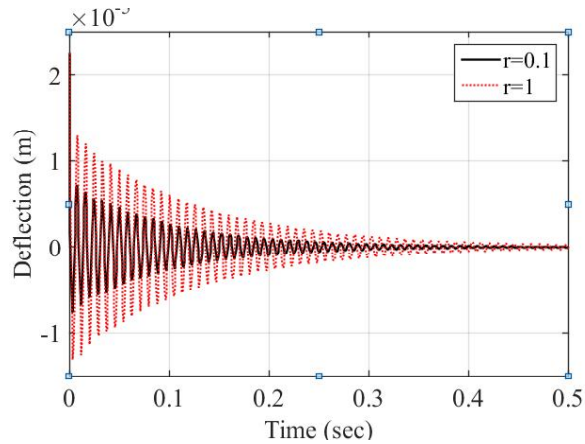

Fig. 7 Effects of LQR controller on higher order model

By increasing the micro-beam stiffness matrix, the higher order model has produced the expected reduction in the maximum amplitude deflections of the micro-beam with respect to classical model. Fig.8 shows the results of the amplitude-frequency response for the modified pair stress micro-beam model and the classical model with an increased frequency range. The reference signal's frequency in this simulation is adjusted to be close to the second mode's linear natural frequency. This figure shows that the displacements for the classical model are larger than the displacements for the higher order at every frequency.

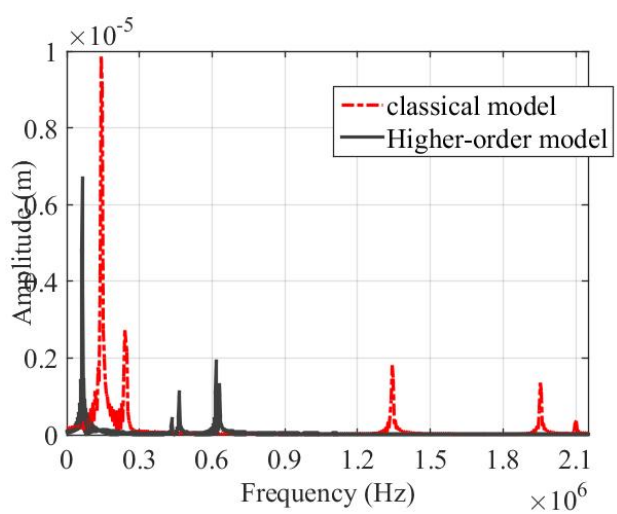

Fig. 8 Frequency to amplitude response comparison of classical and higher order models

5- Conclusion

In this work, the free vibration analysis and dynamic response of higher order model was presented. The variational method was used to derive the governing equations of motion. These equations were then discretized using the GDQ technique. The set of ordinary differential equations was thus created from the set of partial differential equations.

The study's findings suggest that taking into account the independent material length scale parameter will boost the model's stiffness and natural frequency. Natural frequencies are shown to rise nonlinearly with an increase in the value of the material length scale. Furthermore, it was discovered that the natural frequency was predicted more precisely by surface stress conjunctive with higher order theory than by the classical model. It has been observed that the LQR approach, which actively controls vibration in dynamical systems, can significantly reduce vibration. This controlling scheme is a effective tool to reduce the model amplitude and control the shape.

References

[1] Oveissi, S., Toghraie, D. S., & Eftekhari, S. A. (2017). Analysis of transverse vibrational response and instabilities of axially moving CNT conveying fluid. International Journal of Fluid Mechanics Research, 44(2).

[2] Chen, J., Khabaz, M. K., Ghasemian, M. M., Altalbawy, F. M., Jalil, A. T., Eftekhari, S. A., ... & Albahash, Z. F. (2023). Transverse vibration analysis of double-walled carbon nanotubes in an elastic medium under temperature gradients and electrical fields based on nonlocal Reddy beam theory. Materials Science and Engineering: B, 291, 116220.

[3] Al-Shujairi, M., & Mollamahmutoğlu, Ç. (2018). Buckling and free vibration analysis of functionally graded sandwich micro-beams resting on elastic foundation by using nonlocal strain gradient theory in conjunction with higher order shear theories under thermal effect. Composites Part B: Engineering, 154, 292-312..

[4] Zhang, Y., Hammoodi, K. A., Sajadi, S. M., Li, Z., Jasim, D. J., Nasajpour-Esfahani, N., ... & Khabaz, M. K. (2024). Obtaining an accurate prediction model for viscosity of a new nano-lubricant containing multi-walled carbon nanotube-titanium dioxide nanoparticles with oil SAE50. Tribology International, 191, 109185.

[5] Lin, C., Zhou, J., Lu, Q., Khabaz, M. K., Andani, A. K., Al-Yasiri, M., & Pan, G. (2023). Thermal conductivity prediction of WO3-CuO-Ag (35: 40: 25)/water hybrid ternary nanofluid with Artificial Neural Network and back-propagation algorithm. Materials Today Communications, 36, 106807.

[6] Salarnia, M., Toghraie, D., Fazilati, M. A., Mehmandoust, B., & Pirmoradian, M. (2023). The effects of different nanoparticles on physical and thermal properties of water in a copper oscillating heat pipe via molecular dynamics simulation. *Journal of the Taiwan Institute of Chemical Engineers*, *143*, 104721.

[7] Torkan, E., Pirmoradian, M., & Hashemian, M. (2017). Occurrence of parametric resonance in vibrations of rectangular plates resting on elastic foundation under passage of continuous series of moving masses. *Modares Mechanical Engineering*, *17*(9), 225-236.

[8] Balootaki, A. A., Karimipour, A., & Toghraie, D. (2018). Nano scale lattice Boltzmann method to simulate the mixed convection heat transfer of air in a lid-driven cavity with an endothermic obstacle inside. Physica A: Statistical Mechanics and Its Applications, 508, 681-701.

[9] Abdulhameed, M., Muhammad, M. M., Gital, A. Y., Yakubu, D. G., & Khan, I. (2019). Effect of fractional derivatives on transient MHD flow and radiative heat transfer in a micro-parallel channel at high zeta potentials. Physica A: Statistical Mechanics and its Applications, 519, 42-71.

[10] Kong, S., Zhou, S., Nie, Z., & Wang, K. (2008). The size-dependent natural frequency of Bernoulli–Euler micro-beams. International Journal of Engineering Science, 46(5), 427-437.

[11] Kong, S., Zhou, S., Nie, Z., & Wang, K. (2009). Static and dynamic analysis of micro beams based on strain gradient elasticity theory. International Journal of Engineering Science, 47(4), 487-498.

[12] Belardinelli, P., Hauzer, L. M. F. R., Šiškins, M., Ghatkesar, M. K., & Alijani, F. (2018). Modal analysis for density and anisotropic elasticity identification of adsorbates on microcantilevers. Applied Physics Letters, 113(14).

[13] Eringen, A. C., & Edelen, D. (1972). On nonlocal elasticity. International journal of engineering science, 10(3), 233-248.

[14] Saffari, S., Hashemian, M., & Toghraie, D. (2017). Dynamic stability of functionally graded nanobeam based on nonlocal Timoshenko theory considering surface effects. Physica B: Condensed Matter, 520, 97-105.

[15] Alashti, A. R., & Abolghasemi, A. H. (2014). A size-dependent Bernoulli-Euler beam formulation based on a new model of couple stress theory. International Journal of Engineering TRANSACTIONS C, 27(6), 951-960.

[16] Nikpourian, A., Ghazavi, M. R., & Azizi, S. (2019). Size-dependent secondary resonance of a piezoelectrically laminated bistable MEMS arch resonator. Composites Part B: Engineering, 173, 106850.

[17] Jomehzadeh, E., Noori, H. R., & Saidi, A. R. (2011). The size-dependent vibration analysis of micro-plates based on a modified couple stress theory. Physica E: Low-dimensional Systems and Nanostructures, 43(4), 877-883.

[18] Sedighi, H. M., Keivani, M., & Abadyan, M. (2015). Modified continuum model for stability analysis of asymmetric FGM double-sided NEMS: corrections due to finite conductivity, surface energy and nonlocal effect. Composites Part B: Engineering, 83, 117-133.

[19] Ding, N., Xu, X., Zheng, Z., & Li, E. (2017). Size-dependent nonlinear dynamics of a microbeam based on the modified couple stress theory. Acta Mechanica, 228, 3561-3579.

[20] Farokhi, H., Ghayesh, M. H., & Amabili, M. (2013). Nonlinear dynamics of a geometrically imperfect microbeam based on the modified couple stress theory. International Journal of Engineering Science, 68, 11-23.

[21]Sahmani, S., & Bahrami, M. (2015). Size-dependent dynamic stability analysis of microbeams actuated by piezoelectric voltage based on strain gradient elasticity theory. Journal of Mechanical Science and Technology, 29, 325-333.

[22] Lazopoulos, K. A., & Lazopoulos, A. K. (2010). Bending and buckling of thin strain gradient elastic beams. European Journal of Mechanics-A/Solids, 29(5), 837-843.

[23] Trindade, M. A., & Benjeddou, A. (2008). Refined sandwich model for the vibration of beams with embedded shear piezoelectric actuators and sensors. Computers & Structures, 86(9), 859-869.

[24] Ghazavi, M. R., Rezazadeh, G., & Azizi, S. (2010). Pure parametric excitation of a micro cantilever beam actuated by piezoelectric layers. Applied Mathematical Modelling, 34(12), 4196-4207.

[25] AkhavanAlavi, S. M., Mohammadimehr, M., & Edjtahed, S. (2019). Active control of micro Reddy beam integrated with functionally graded nanocomposite sensor and actuator based on linear quadratic regulator method. European Journal of Mechanics-A/Solids, 74, 449-461.

[26] Belardinelli, P., Sajadi, B., Lenci, S., & Alijani, F. (2019). Global dynamics and integrity of a micro-plate pressure sensor. Communications in Nonlinear Science and Numerical Simulation, 69, 432-444.

[27]Mohammadimehr, M., Mohammadi Hooyeh, H., Afshari, H., & Salarkia, M. R. (2017). Free vibration analysis of double-bonded isotropic piezoelectric Timoshenko microbeam based on strain gradient and surface stress elasticity theories under initial stress using differential quadrature method. Mechanics of Advanced Materials and Structures, 24(4), 287-303.

[28] Mirkalantari, S. A., Hashemian, M., Eftekhari, S. A., & Toghraie, D. (2017). Pull-in instability analysis of rectangular nanoplate based on strain gradient theory considering surface stress effects. Physica B: Condensed Matter, 519, 1-14.

[29] Eftekhari, S. A., Hashemian, M., & Toghraie, D. (2020). Optimal vibration control of multi-layer micro-beams actuated by piezoelectric layer based on modified couple stress and surface stress elasticity theories. Physica A:

Statistical Mechanics and its Applications, 546, 123998.

[30]Eftekhari, S. A., & Toghraie, D. (2022). Vibration and dynamic analysis of a cantilever sandwich microbeam integrated with piezoelectric layers based on strain gradient theory and surface effects. Applied Mathematics and Computation, 419, 126867.

[31]Pirmoradian, M., & Karimpour, H. (2017). Nonlinear effects on parametric resonance of a beam subjected to periodic mass transition. *Modares Mechanical Engineering*, *17*(1), 284-292.

[32] Arani, A. G., Abdollahian, M., & Kolahchi, R. (2015). Nonlinear vibration of a nanobeam elastically bonded with a piezoelectric nanobeam via strain gradient theory. International Journal of Mechanical Sciences, 100, 32-40.

[33]Eftekhari, S. A., & Toghraie, D. (2022). Vibration and dynamic analysis of a cantilever sandwich microbeam integrated with piezoelectric layers based on strain gradient theory and surface effects. Applied Mathematics and Computation, 419, 126867.

[34]Mohammadimehr, M., Mohammadi Hooyeh, H., Afshari, H., & Salarkia, M. R. (2017). Free vibration analysis of double-bonded isotropic piezoelectric Timoshenko microbeam based on strain gradient and surface stress elasticity theories under initial stress using differential quadrature method. Mechanics of Advanced Materials and Structures, 24(4), 287-303.

[35] Keivani, M., Koochi, A., Kanani, A., Mardaneh, M. R., Sedighi, H. M., & Abadyan, M. (2017). Using strain gradient elasticity in conjunction with Gurtin–Murdoch theory for modeling the coupled effects of surface and size phenomena on the instability of narrow nano-switch. Proceedings of the Institution of Mechanical Engineers, Part C: Journal of Mechanical Engineering Science, 231(17), 3277-3288.

[36] Pirmoradian, M., Naeeni, H. A., Firouzbakht, M., Toghraie, D., & Darabi, R. (2020). Finite element analysis and experimental evaluation on stress distribution and sensitivity of dental implants to assess optimum length and thread pitch. Computer methods and Programs in Biomedicine, 187, 105258.

[37] Hejazi, S. A. M., Feyzpour, A., Eslami, A., Fouladgar, M., Eftekhari, S. A., & Toghraie, D. (2023). Numerical investigation of rigidity and flexibility parameters effect on superstructure foundation behavior using three-dimensional finite element method. Case Studies in Construction Materials, 18, e01867.

[38] Chen, J., Khabaz, M. K., Ghasemian, M. M., Altalbawy, F. M., Jalil, A. T., Eftekhari, S. A., ... & Albahash, Z. F. (2023). Transverse vibration analysis of double-walled carbon nanotubes in an elastic medium under temperature gradients and electrical fields based on nonlocal Reddy beam theory. Materials Science and Engineering: B, 291, 116220.

[39] Abdi, F., Ghasemi, A., Ariaei, A., Eftekhari, S. A., Nasr, M., Khabaz, M. K., & Salahshour, S. (2025). Free vibration and buckling analysis of axially functionally graded tapered Timoshenko beams using B-spline-based isogeometric analysis. Heliyon, 11(1).